

Symmetry-breaking vortex-lattice of a binary superfluid in a rotating bucket

S. K. Adhikari

Instituto de Física Teórica, Universidade Estadual Paulista - UNESP, 01.140-070 São Paulo, São Paulo, Brazil

Abstract

We study spontaneous-symmetry-broken phase-separated vortex lattice in a weakly interacting *uniform* rapidly rotating binary Bose superfluid contained in a quasi-two-dimensional circular or square bucket. For the inter-species repulsion above a critical value, the two superfluid components separate and form a demixed phase with practically no overlap in the vortex lattices of the two components, which will permit an efficient experimental observation of such vortices and study their properties. In case of a circular bucket with equal intra-species energies of the two components, the two components separate into two non-overlapping semicircular domains for all frequencies of rotation Ω generating distinct demixed vortex lattices. In case of a binary Bose superfluid in both circular and square buckets, (a) the number of vortices increases linearly with Ω in agreement with a suggestion by Feynman, and (b) the rotational energy in the rotating frame decreases quadratically with Ω in agreement with a suggestion by Fetter.

Keywords: Rotating binary Bose-Einstein condensate, Vortex lattice, Mean-field model; Phase separation, Spontaneous symmetry breaking

1. Introduction

The formation of a regular lattice of quantized vortices in a uniform superfluid under rotation signals its superfluid nature. The integral of the velocity field \mathbf{v} around a generic closed path C in a rotating superfluid is quantized [1, 2, 3, 4]:

$$\oint_C \mathbf{v} \cdot d\mathbf{r} = 2\pi\hbar l/m, \quad (1)$$

where m is the mass of an atom in the superfluid, the associated angular momentum l of a is zero or an integer (for a quantized vortex) and m is the mass of an atom. A rapidly rotating uniform superfluid prefers many vortices of unit angular momentum arranged in a regular lattice, often a triangular lattice, over a vortex of multiple angular momentum [3]. Quantized vortices of unit angular momentum were first observed in a uniform superfluid He II in a rotating bucket [5, 6]. Soon after the observation of a trapped dilute weak-coupling Bose-Einstein condensate (BEC) in alkali-metal atoms in a laboratory [7], a single vortex [8] and hundreds of vortices [9] arranged in Abrikosov triangular lattice in a rapidly rotating harmonically-trapped superfluid BEC were observed under controlled conditions and studied theoretically [10] using the weak-coupling mean-field Gross-Pitaevskii (GP) equation [11].

More recently it has been possible to create a BEC in a laboratory in a one- [12] and a multi-dimensional [13] optical box trap so that the condensate is subjected to a uniform potential inside the box. The optical trap considered in Ref. [13] is a uniform three-dimensional cylindrical box trap which combines a circular box trap in the $x-y$ plane and a one-dimensional confinement in the z direction which is really the bucket of rotating He II experiments [5, 6]. It has been demonstrated that a rapidly rotating quasi-two-dimensional (quasi-2D) uniform scalar BEC in circular and square buckets can form a variety of vortex lattice structures including triangular and square lattices [14]. With this experimental possibility of realizing a uniform dilute BEC in a bucket, in this Letter, we set to study vortex generation in a dilute uniform rapidly rotating quasi-2D binary BEC in a circular or a square bucket. Recently, we studied triangular vortex lattice generation in a binary BEC in a harmonic trap [15].

The number of vortices in a rapidly rotating large uniform superfluid increases linearly with the angular frequency of rotation Ω according to a suggestion of Feynman. In a harmonically trapped rotating BEC, this linear relation is grossly violated with the number of vortices rapidly increasing as Ω approaches the trapping frequency [4]. Similarly, Fetter suggested using general

considerations that the Ω -dependent rotational energy of a single-component uniform superfluid in a bucket is the rotational energy of rigid-body rotation of the superfluid with the corresponding moment of inertia and is proportional to Ω^2 . We find that both these laws, e.g., the linear increase of the number of vortices with Ω and quadratic decrease of the rotational energy with Ω , are also valid in the present case of a rotating uniform binary BEC.

The study of vortex lattices in a binary or a multi-component spinor BEC is interesting because it may lead to the formation of square [14, 16, 17], stripe [14] and honeycomb [18] vortex lattices, other than the standard Abrikosov triangular lattice [3], in addition to coreless vortices [19], vortices of fractional charge [20], and phase-separated vortex lattices in multi-component non-spinor [21] and dipolar [17] BECs. The difficulty of experimental study of overlapping vortices in different components of a multi-component BEC is monumental and despite great interest [22, 23], there are only a few experimental studies [16, 24] on vortex lattices in a rotating binary BEC. Hence it will be highly desirable to have phase-separated vortex lattices in a binary BEC, where the vortices and component density of one component do not overlap with those of the other. In this Letter, we investigate the possibility of generating phase-separated triangular, circular and square vortex lattice structure in a binary rotating BEC confined in a square or a circular bucket.

In a repulsive uniform binary BEC, phase separation takes place for [25]

$$\kappa \equiv \frac{g_1 g_2}{g_{12}^2} < 1, \quad (2)$$

where g_1 and g_2 are intra-species repulsion strengths for components 1 and 2, respectively, and g_{12} inter-species repulsion strength. We find that the parameter domain leading to completely phase-separated vortex lattices in a rotating quasi-2D binary BEC is governed by condition (2) so that the vortices of one component do not have any overlap with the matter density of the other component. We find that if $g_1 = g_2$ and $\kappa < 1$, then for a circular rotating bucket the phase separated components may have the form of completely non-overlapping semi-circles lying opposite to each other spontaneously breaking the circular symmetry of the underlying Lagrangian. In presence of rotation, the vortices are formed on the phase-separated semicircular components. In case of a square bucket with $g_1 = g_2$ the phase-separated components have the form of adjacent rectangles spontaneously breaking the symmetry of the underlying Lagrangian. In case $g_1 \neq g_2$ and $\kappa < 1$, for a quasi-2D BEC in a circular bucket there will be

complete phase separation between components with irregular shape and upon rotation, vortices are formed on phase separated components with spontaneous symmetry breaking. This will facilitate the experimental observation and consequent studies of vortex lattices in binary BEC where the vortex lattice of one component has no overlap with the other component. It is worthwhile to point out that none of the previous studies on rotating binary BEC, identified vortex lattice in a phase-separated phase. In all previous studies overlapping configuration of the two components were considered.

2. Mean-field model for a rapidly rotating binary BEC

A dilute BEC of N atoms of mass m each in the weak-coupling limit at zero temperature is described by the following mean-field GP equation [11]

$$i\hbar \frac{\partial \phi(\mathbf{r}, t)}{\partial t} = \left[-\frac{\hbar^2}{2m} \nabla^2 + V(\mathbf{r}) + \frac{4\pi\hbar^2 a}{m} n \right] \phi(\mathbf{r}, t) \quad (3)$$

where a is the scattering length of atoms, density $n = N|\phi(\mathbf{r}, t)|^2$, and normalization $\int d\mathbf{r} |\phi(\mathbf{r}, t)|^2 = 1$, and N the number of atoms.

We will describe a binary rotating uniform BEC in a cylindrical or square bucket in a similar fashion using a generalization of the GP equation (3) for the binary system [21, 26]. The GP equation has been well tested in the generation of vortices in a harmonically trapped (non-uniform) single component [10] and binary [16, 24, 27] BEC. Now it is possible to make a binary BEC of two hyper-fine states of the same atomic species, such as ^{39}K and ^{87}Rb atoms. In such cases the masses of the two species are equal. Thus in this theoretical study we will take the masses of two species to be equal. The study of a rapidly rotating binary BEC is conveniently performed in the rotating frame, where the generated vortex lattice is a stationary state [4], which can be obtained by the imaginary-time propagation method [28]. Such a dynamical equation in the rotating frame can be written if we note that the Hamiltonian in the rotating frame is given by [29] $H = H_0 - \Omega l_z$, where H_0 is that in the laboratory frame, l_z is the z component of angular momentum given by $l_z = i\hbar(y\partial/\partial x - x\partial/\partial y)$. With the inclusion of the extra rotational energy $-\Omega l_z$ in the Hamiltonian, the coupled GP equations for the binary BEC in the rotating frame

can be written as [21, 26]

$$i\hbar \frac{\partial \phi_1(\mathbf{r}, t)}{\partial t} = \left[-\frac{\hbar^2}{2m} \nabla^2 + V(\mathbf{r}) - \Omega l_z + \frac{4\pi\hbar^2}{m} \left\{ a_1 N_1 \right. \right. \\ \left. \left. \times |\phi_1(\mathbf{r}, t)|^2 + a_{12} N_2 |\phi_2(\mathbf{r}, t)|^2 \right\} \right] \phi_1(\mathbf{r}, t), \quad (4)$$

$$i\hbar \frac{\partial \phi_2(\mathbf{r}, t)}{\partial t} = \left[-\frac{\hbar^2}{2m} \nabla^2 + V(\mathbf{r}) - \Omega l_z + \frac{4\pi\hbar^2}{m} \left\{ a_2 N_2 \right. \right. \\ \left. \left. \times |\phi_2(\mathbf{r}, t)|^2 + a_{12} N_1 |\phi_1(\mathbf{r}, t)|^2 \right\} \right] \phi_2(\mathbf{r}, t), \quad (5)$$

where the two species of atoms are denoted $i = 1, 2$, $\phi_i(\mathbf{r}, t)$ are the order parameters of the two components, N_i is the number of atoms in species i , $\mathbf{r} = \{x, y, z\}$, a_i is the intra-species scattering length of species i , a_{12} is the inter-species scattering length. The functions ϕ_i are normalized as $\int d\mathbf{r} |\phi_i(\mathbf{r}, t)|^2 = 1$.

The following dimensionless form of Eqs. (4) and (5) can be obtained by the transformation of variables: $\mathbf{r}' = \mathbf{r}/l_0$, $t' = t\omega$, $\phi'_i = \phi_i l_0^{3/2}$, $\Omega' = \Omega/\omega$, $l'_z = l_z/\hbar$, $\omega = \hbar/ml_0^2$, with l_0 a scaling length [21]:

$$i \frac{\partial \phi_1(\mathbf{r}, t)}{\partial t} = \left[-\frac{\nabla^2}{2} + V(\mathbf{r}) - \Omega l_z + 4\pi N_1 a_1 |\phi_1|^2 \right. \\ \left. + 4\pi a_{12} N_2 |\phi_2|^2 \right] \phi_1(\mathbf{r}, t), \quad (6)$$

$$i \frac{\partial \phi_2(\mathbf{r}, t)}{\partial t} = \left[-\frac{\nabla^2}{2} + V(\mathbf{r}) - \Omega l_z + 4\pi N_2 a_2 |\phi_2|^2 \right. \\ \left. + 4\pi a_{12} N_1 |\phi_1|^2 \right] \phi_2(\mathbf{r}, t), \quad (7)$$

where for simplicity we have dropped the prime from the transformed variables.

We assume that the extension of the binary BEC mixture in the z direction is limited between $z = \pm z_0$ due to strong trapping in this direction and the density in the z direction is integrable. The order parameter can then be written as $\phi_i(\mathbf{r}) = \psi_i(\boldsymbol{\rho}, t) \Phi_i(z)$, where the function $\psi_i(\boldsymbol{\rho}, t)$ carries the essential dynamics and $\Phi_i(z)$ is normalizable between $z = \pm z_0$: $\int_{-z_0}^{z_0} dz |\Phi_i(z)|^2 = \mathcal{N}_i$. For a strong harmonic trap in the z direction $z_0 \rightarrow \infty$ and $\Phi_i(z)$ has the form of a Gaussian: the ground state in the harmonic trap. In that case the z dependence in Eqs. (6) and (7) can be integrated out [30] and we have the following quasi-2D equations

$$i \frac{\partial \psi_1(\boldsymbol{\rho}, t)}{\partial t} = \left[-\frac{\nabla_{\boldsymbol{\rho}}^2}{2} + V(\boldsymbol{\rho}) - \Omega l_z + g_1 |\psi_1|^2 \right. \\ \left. + g_{12} |\psi_2|^2 \right] \psi_1(\boldsymbol{\rho}, t), \quad (8)$$

$$i \frac{\partial \psi_2(\boldsymbol{\rho}, t)}{\partial t} = \left[-\frac{\nabla_{\boldsymbol{\rho}}^2}{2} + V(\boldsymbol{\rho}) - \Omega l_z + g_2 |\psi_2|^2 \right. \\ \left. + g_{21} |\psi_1|^2 \right] \psi_2(\boldsymbol{\rho}, t), \quad (9)$$

where $\boldsymbol{\rho} = \{x, y\}$, $\rho^2 = x^2 + y^2$, $g_i = 4\pi a_i N_i \mathcal{M}_i / \mathcal{N}_i$, $g_{12} = 4\pi a_{12} N_2 \mathcal{M}_{12} / \mathcal{N}_1$, $g_{21} = 4\pi a_{12} N_1 \mathcal{M}_{12} / \mathcal{N}_2$,

$\int_{-z_0}^{z_0} dz |\Phi_i(z)|^4 = \mathcal{M}_i$ and $\int_{-z_0}^{z_0} dz |\Phi_1(z)|^2 |\Phi_2(z)|^2 = \mathcal{M}_{12}$. In this study we will take $g_{12} = g_{21}$ maintaining the possibility $g_1 \neq g_2$. Equations (8) and (9) are the mean-field GP equations for the quasi-2D rotating binary BEC in a bucket. For a circular quasi-2D bucket of radius \mathcal{R}

$$V(\boldsymbol{\rho}) = 0, \quad \rho < \mathcal{R}, \quad (10)$$

$$V(\boldsymbol{\rho}) \rightarrow \infty, \quad \rho > \mathcal{R}, \quad (11)$$

and for a square bucket of length d

$$V(\boldsymbol{\rho}) = 0, \quad |x|, |y| < d/2, \quad (12)$$

$$V(\boldsymbol{\rho}) \rightarrow \infty, \quad |x|, |y| > d/2. \quad (13)$$

The binary GP equations (8) and (9) can also be obtained using a variational procedure:

$$i \frac{\partial \psi_i(\boldsymbol{\rho}, t)}{\partial t} = \frac{\delta E}{\delta \psi_i^*(\boldsymbol{\rho}, t)} \quad (14)$$

with the following energy functional in the rotating frame:

$$E(\Omega) = \frac{1}{2} \int d\boldsymbol{\rho} \left[\sum_i \frac{1}{2} \left(|\nabla_{\boldsymbol{\rho}} \psi_i|^2 + 2V(\boldsymbol{\rho}) |\psi_i|^2 + g_i |\psi_i|^4 \right. \right. \\ \left. \left. - 2\psi_i^* l_z \Omega \psi_i \right) + g_{12} |\psi_1|^2 |\psi_2|^2 \right]. \quad (15)$$

This energy functional is essentially the average energy of a single atom in the symmetric case: $N_1 = N_2$. We note that the rotational energy $\int d\boldsymbol{\rho} \psi_i^* l_z \Omega \psi_i$ is positive. Hence the energy E in the rotating frame will decrease with the increase of angular frequency of rotation. All other contributions to energy (15) are positive. The contribution of the rotational energy will be [4] proportional to Ω^2 and the energy will decrease quadratically with Ω .

3. Numerical Results

To solve Eqs. (8) and (9) numerically, we propagate these equations in time by the split time-step Crank-Nicolson discretization scheme [28, 31] using a space step of 0.05 and a time step of 0.0002 for imaginary-time simulation and 0.0001 for real-time simulation, respectively, to obtain the stationary state and to study the dynamics. There are different C and FORTRAN programs for solving the GP equation [28, 31] and one should use the appropriate one. These programs have recently been adapted to simulate the vortex lattice in a rapidly rotating BEC [32] and we use these in this study. In this Letter, without considering a specific atom, we will present the results in dimensionless units for different sets of parameters: $\Omega, g_1, g_2, g_{12}(=g_{21})$. In

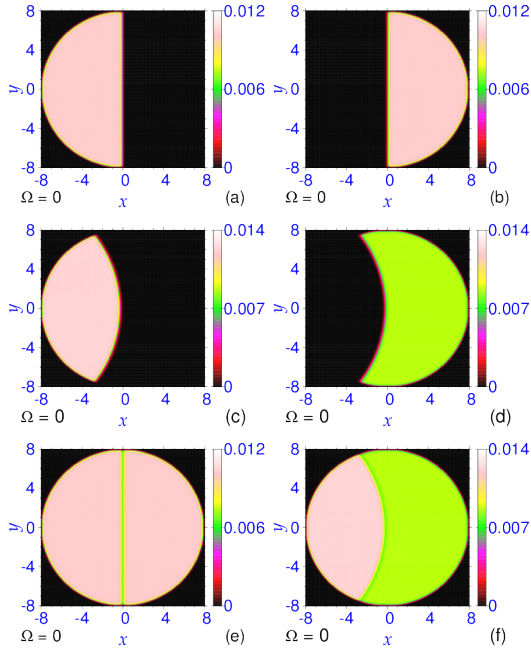


Figure 1: Phase separation in a non-rotating ($\Omega = 0$) quasi-2D binary BEC in a circular bucket from a contour plot of 2D densities ($|\psi_i|^2$): (a) first and (b) second components for $g_1 = g_2 = 5000, g_{12} = 10000$, (c) first and (d) second components for $g_1 = 5000, g_2 = g_{12} = 10000$. The densities of the two components together for $g_1 = g_2 = 5000$ and for $g_1 = 5000, g_2 = 10000$ are shown in (e) and (f), respectively. All quantities plotted in this and following figures are dimensionless.

the phenomenology of a specific atom, the parameters g_1, g_2, g_{12} can be varied experimentally through a variation of the underlying intra- and inter-species scattering lengths by the Feshbach resonance technique [33].

We demonstrate a phase separation in a fully repulsive ($g_i, g_{12} > 0$) non-rotating quasi-2D binary BEC ($\Omega = 0$) in a circular bucket. We find that a phase separation follows condition (2). We consider two distinct cases $g_1 = g_2$ and $g_1 \neq g_2$. To illustrate these cases we consider (i) $g_1 = g_2 = 5000, g_{12} = 10000$ and (ii) $g_1 = 5000, g_2 = g_{12} = 10000$ in dimensionless units, both satisfying condition (2). All numbers reported in this Letter are in dimensionless units. In the first case, the densities of the first and the second components are shown in Figs. 1(a) and (b), respectively. In this case, there is a complete phase separation with the two components occupying two self-avoiding semi circles. In the second case, the densities of the first and the second components are shown in Figs. 1(c) and (d), respectively. In this case, there is also a complete phase separation, but with the two components occupying different areas. As $g_2 > g_1$, the second component occupies

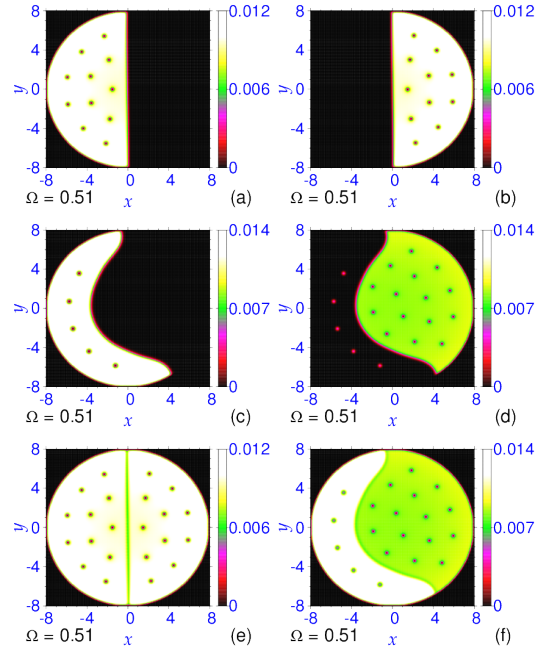


Figure 2: Same as in Fig. 1 for a rotating quasi-2D binary BEC for angular frequency $\Omega = 0.51$.

a larger area. In Figs. 1(e) and (f) the densities of the two components for cases (i) and (ii) are displayed together in the same plot. In the first case in Fig. 1(e) the interphase between the two components is indicated by a lowering of density. In the second case in Fig. 1(f) the two component densities are very different and the interphase between the two components can be easily identified. This kind of phase separation breaks the circular symmetry of the system and this symmetry breaking continues in presence of rapid rotation with vortex generation.

In Figs. 2(a)-(d) we plot the component densities of a rotating quasi-2D binary BEC in a circular bucket with angular frequency of rotation $\Omega = 0.51$ with same interaction parameters g_1, g_2, g_{12} as the non-rotating BECs considered in Figs. 1(a)-(d). In the symmetric case illustrated in Figs. 2(a)-(b) ($g_1 = g_2$), the components maintain the phase-separated semicircular shapes as in Figs. 1(a)-(b). Under rotation the same number of vortices has appeared in Figs. 2(a)-(b) ($11+11=22$). However, the numbers of vortices in the two components could be different for a general arbitrary Ω . In the asymmetric case shown in Figs. 2(c)-(d), the two components remain phase separated, but the shapes of individual components have changed when compared with those of Figs. 1(c)-(d), where different numbers of vor-

tices ($5+15=20$) have appeared in the two components. The change of shape of the two component densities in Figs. 2(c)-(d) upon rotation is due to the nonuniform centrifugal force acting on the two components. The average distance of the center of mass of the first component from the center, viz. Fig. 1(c), is larger than that of the second component from the center, viz. Fig. 1(d) resulting in a larger centrifugal force on the former upon rotation. Hence the first component is squeezed more than the second component upon rotation due to a larger centrifugal acceleration, resulting in an inner concavity of the first component and a convexity of the second. In Figs. 1(a)-(b) the sizes of the two components are same and subject to the same centrifugal force. Hence their shapes do not change upon rotation. In Figs. 2(e)-(f), as in Figs. 1(e)-(f), we have illustrated both components of the rotating binary mixture in the same plot. Again, as in the non-rotating case, it is easy to identify the two self avoiding components with multiple vortices in these combined plots. Hence for a compact presentation, we will exhibit the two component densities of the rotating binary mixture in the same plot in the following. Often due to atomic repulsion, quite naturally, the vortex core of one component is filled with atoms of the other component, as can be seen prominently in Fig. 2(d).

Now we study how the number of vortices evolve with the increase of angular frequency of rotation Ω in the symmetric case $g_1 = g_2 = 5000$ with $g_{12} = 10000$. We consider a large g_{12} , as for a large g_{12} , the phase separation is robust, leading to a ground state with phase-separated vortex lattice. For $g_{12} \gtrsim g_1 = g_2$, there is a phase separation, and the ground state of a harmonically trapped binary BEC has a phase-separated sheet structure [18, 23]. In Figs. 3(a)-(f) we display the fully phase-separated vortex-lattice states with increasing angular frequency of rotation: $\Omega =$ (a) 0.4, (b) 0.6, (c) 0.8, (d) 1.0, (e) 1.2 and (f) 1.4. The corresponding total number of vortices in the two components are (a) 15 ($=7+7$), (b) 26 ($=13+13$), (c) 30 ($=15+15$), (d) 40 ($=20+20$), (e) 47 ($=24+23$), and (f) 60 ($=30+30$); the numbers in the parenthesis are the numbers of vortices in the first and the second components, respectively. The separation between the two components can be clearly seen in this figure in a domain of low density between the two components. The maximum density in the plots in Figs. 3 increases with Ω . We could also find for $\Omega = 1.2$ two states with $(23+23)$ and $(24+24)$ vortices. But these states have energies greater than the $(24+23)$ vortex state shown in Fig. 3(e) and hence are excited states. The energy of a vortex-lattice state depends on the number of vortices as well as their arrangement in space. The vortices in Figs. 3 are ar-

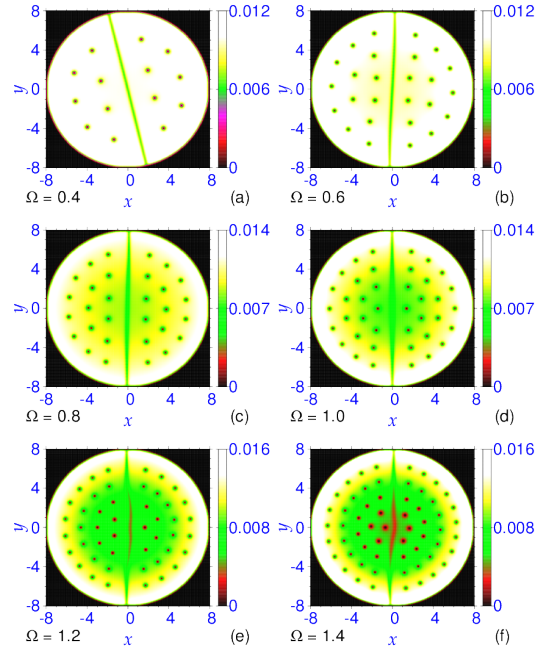


Figure 3: Phase-separated vortex lattices in a rapidly rotating quasi-2D binary BEC in a circular bucket with $g_1 = g_2 = 5000$, $g_{12} = 10000$ for $\Omega =$ (a) 0.4, (b) 0.6, (c) 0.8, (d) 1.0, (e) 1.2, and (f) 1.4 from a contour plot of 2D densities ($|\psi_i|^2$).

ranged in successive orbits around the center, the outer orbits are mostly circular. In a rotating harmonically-trapped binary BEC the vortices are arranged in triangular lattice [15]. Although, the nonlinearities g_i of the two components are the same, the number of vortices in the two components and the arrangement of vortices in the two components could be different. In plots of Figs. 3(a)-(d) and (f) the two components have the same number of vortices; in (e) the numbers of vortices in the two components are different. The arrangements of the vortices in the two components are also the same in (a)-(d), whereas the same is different in (f). Numerically we also identified for $\Omega = 1.4$ another degenerate ground state with the same number of vortices (30) in the two components but with the arrangement of vortices exchanged in the two components in relation to plot (f).

Next we consider the evolution of the number of vortices with the increase of angular frequency of rotation Ω in the asymmetric case ($g_1 \neq g_2$) with $g_1 = 5000$ and $g_2 = g_{12} = 10000$. With these values of g_i and g_{12} the phase separation is very stable. In Figs. 4(a)-(h) we display the fully phase-separated vortex-lattice states with increasing angular frequency of rotation: $\Omega =$ (a) 0.4,

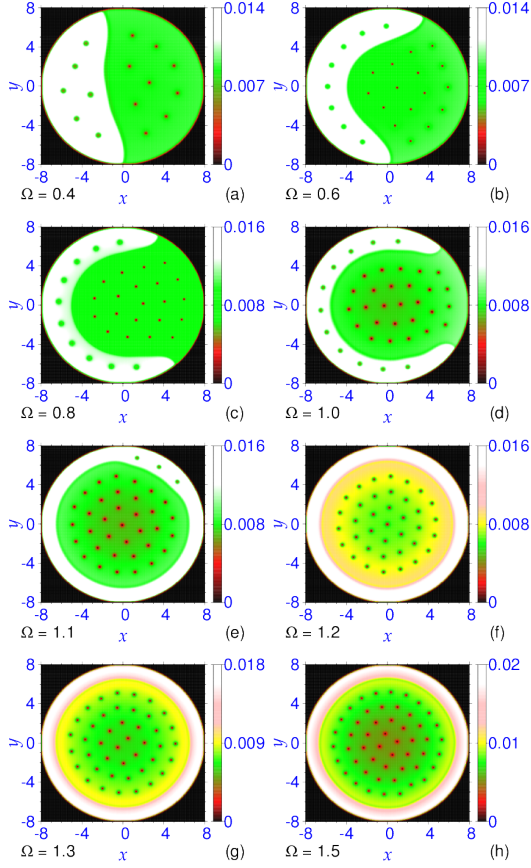


Figure 4: Phase-separated vortex lattices in a rapidly rotating quasi-2D binary BEC in a circular bucket with $g_1 = 5000$, $g_2 = g_{12} = 10000$ for $\Omega =$ (a) 0.4, (b) 0.6, (c) 0.8, (d) 1.0, (e) 1.1, (f) 1.2, (g) 1.3 and (h) 1.5, from a contour plot of 2D densities ($|\psi_i|^2$). The light (pink,white) colored domain is the first component, whereas the dark (green,yellow) colored region is the second component. For a comprehensive presentation of the plots with changing density, the color scheme for plots (a)-(e) is different from plots (f)-(h).

(b) 0.6, (c) 0.8, (d) 1.0, (e) 1.1, (f) 1.2, (g) 1.3 and (h) 1.5. The corresponding total number of vortices in the two components are (a) 15 (=6+9), (b) 24 (=8+16), (c) 31 (=10+21), (d) 38 (=11+27), (e) 38 (=3+35), (f) 37 (=0+37), (g) 43 (=0+43) and (h) 51 (0+51); again the numbers in the parenthesis are the numbers in the first and the second components, respectively. The number of vortices in the first component increases with Ω up to about $\Omega \approx 1$. The first component surrounds the second component more and more as Ω increases to about $\Omega \approx 1$. Beyond $\Omega = 1$ the first component surrounds the second component completely in the form of a ring around the second component occupying an inner circle and the number of vortices in the first component

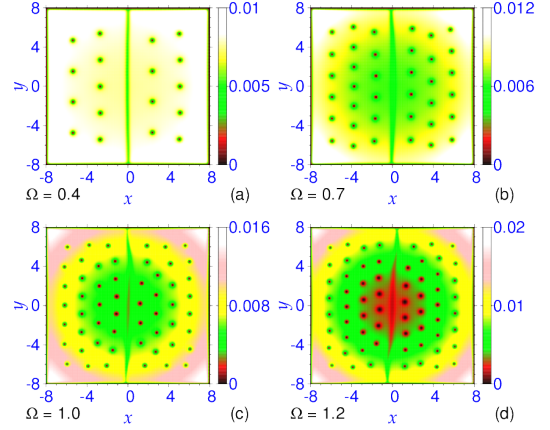


Figure 5: Phase-separated vortex lattices in a rapidly rotating quasi-2D binary BEC in a square bucket with $g_1 = g_2 = 5000$, $g_{12} = 10000$ for $\Omega =$ (a) 0.4, (b) 0.7, (c) 1.0, and (d) 1.2, from a contour plot of 2D densities ($|\psi_i|^2$). For a comprehensive presentation of the plots with changing density, the color scheme for plots (a)-(b) is different from plots (c)-(d).

becomes 0 in the ground state. Between $\Omega \approx 1.0$ and $\Omega \approx 1.2$ the total number of vortices remain fixed approximately at 37, beyond which the number of vortices in the second component increases with Ω whereas that in the first component remains 0. The circular symmetry is broken for small Ω and is restored for $\Omega \gtrsim 1.2$. In this study we displayed the lowest-energy ground states of the system. Imaginary-time simulation for $\Omega > 1.2$ may lead to states with a few vortices in the first component. These states have higher energy and are discarded. The vortices are arranged in successive orbits in plots of Figs. 4(e)-(h). The outer orbits have the shape of circles whereas the inner orbits have the shape of polygons. In case of a harmonically trapped BEC, similar orbits have the shape of hexagons [32] accommodating 1, 6, 12, 18, 24 ... vortices in successive orbits. In (h) the central spot at the origin does not have a vortex, while in (e) and (f) there is a vortex at the center. In (f) the numbers of vortices in successive orbits are 1, 6, 12, 18, as in closed hexagonal orbits [32].

The phase separation with symmetry breaking of a rapidly rotating quasi-2D binary BEC in a square bucket is studied next for $g_1 = g_2 = 5000$ and $g_{12} = 10000$. In Figs. 5(a)-(d) we display the phase-separated vortex-lattice states for angular frequencies $\Omega =$ (a) 0.4, (b) 0.7, (c) 1.0, and (d) 1.2. The corresponding total number of vortices in the two components are (a) 18 (=9+9), (b) 37 (=19+18), (c) 55 (=27+28), (d) 64 (=32+32), respectively. The number of vortices in the two components are the same in (a), and (d) and different in (b) and (c).

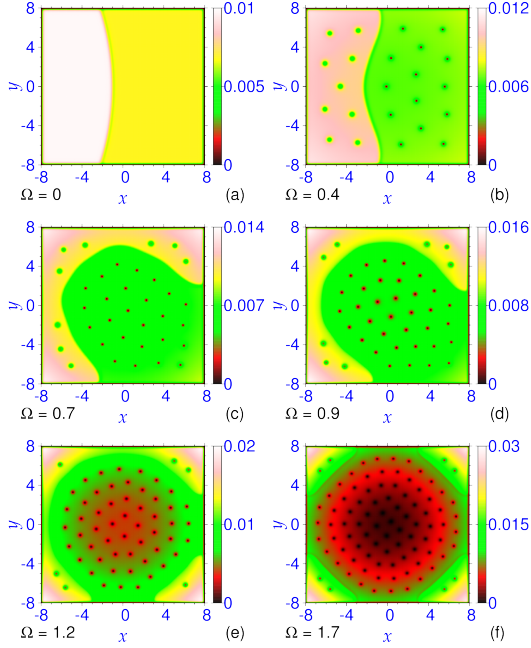


Figure 6: Phase-separated vortex lattices in a rapidly rotating quasi-2D binary BEC in a square bucket with $g_1 = 5000, g_2 = g_{12} = 10000$ for $\Omega =$ (a) 0.4, (b) 0.7, (c) 1.0, and (d) 1.2, from a contour plot of 2D densities ($|\psi_i|^2$). For a comprehensive presentation of the plots with changing density, the color scheme for plots (a)-(b) is different from plots (c)-(d).

Except near the boundary the vortices are arranged in triangular lattice in all plots. In this case the number of vortices also increases with Ω .

Next we investigate the phase separation of a rapidly rotating quasi-2D binary BEC in an asymmetric square bucket for $g_1 = 5000$ and $g_2 = g_{12} = 10000$. In Figs. 6(a)-(f) we display the phase-separated vortex-lattice states for angular frequencies $\Omega =$ (a) 0, (b) 0.4, (c) 0.7, (d) 0.9, (e) 1.2, and (f) 1.7. The corresponding total number of vortices in the two components are (a) 0, (b) 23 (=9+14), (c) 35 (=9+26), (d) 43 (=8+35), (e) 59 (=6+53), (f) 92 (=8+84), respectively. The total number of vortices increase with Ω . In the central region the vortices are arranged in approximate triangular lattice.

The number of vortices in a rotating BEC in a bucket can be obtained from a theoretical estimate of Feynman [2]. For a large number of vortices, the areal density of vortices (number of vortices per unit area) tends to

$$\mathcal{N} = \frac{\Omega}{\pi} \quad (16)$$

in units $\hbar = m = 1$. Hence the number of vortices in a

circular area of radius \mathcal{R} is

$$N_{\text{circle}} = \mathcal{R}^2 \Omega, \quad (17)$$

and that in a square of side d is

$$N_{\text{square}} = \frac{d^2 \Omega}{\pi}. \quad (18)$$

The Feynman estimates for generated vortices (17) and (18) are proportional to Ω and give an idea about the number of vortices in an actual numerical calculation.

The Ω -dependent part of energy per atom can be obtained from a theoretical estimate of Fetter [4]:

$$E(\Omega) - E(0) = -\frac{1}{2} I \Omega^2, \quad (19)$$

where I is the moment of inertia of rigid-body rotation of an atom of the superfluid. For a quasi-2D BEC atom of mass $m = 1$, the moment of inertia of a circle of radius \mathcal{R} is $\mathcal{R}^2/2$ and that of a uniform square of side d is $d^2/6$. Hence the Fetter estimates of Ω -dependent energies per atom of a BEC in a circular and square buckets are, respectively

$$E(\Omega) - E(0) = -\frac{\mathcal{R}^2 \Omega^2}{4} \quad (20)$$

$$E(\Omega) - E(0) = -\frac{d^2 \Omega^2}{12}. \quad (21)$$

In case of the square, the estimate is applicable in the symmetric case only ($g_1 = g_2$), where the density is uniform, and not in the asymmetric case ($g_1 \neq g_2$) of nonuniform density.

In Figs. 7(a)-(b) we plot the numerically obtained number of vortices and the Ω -dependent energy in the rotating frame versus Ω , respectively, for a rotating quasi-2D binary BEC in a circular bucket. We also plot the theoretical estimates of Feynman [2] (17) for the number of vortices and of Fetter [4] (20) for the Ω -dependent part of energy in the rotating frame. As expected, the number of vortices increases with Ω and energy decreases as Ω is increased. The energy decreases as the contribution of the rotational energy $-\Omega l_z$ in the expression for energy (15) is negative. In the asymmetric case around $\Omega \sim 1.0$ to 1.2, the first component forms a thin ring around the second component. Because of the small width of the first component it cannot accommodate any vortex. Thus the number of vortices in the first component reduces to zero and this volume is excluded from vortex formation, while the number of vortices in the second component continue to increase, so that the total number vortices remain constant, viz. Fig. 7(a). As Ω is further increased beyond $\Omega = 1.2$ the

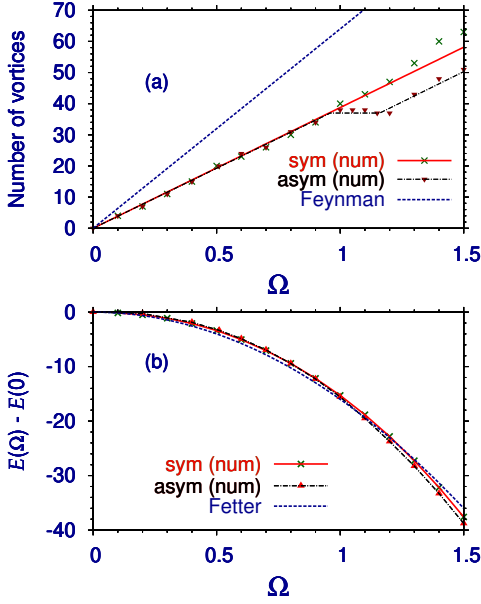


Figure 7: (a) Number of vortices and (b) energy $E(\Omega) - E(0)$ in the rotating frame for a rapidly rotating quasi-2D binary BEC in a circular bucket versus angular frequency of rotation Ω for (i) the symmetric (sym) case with $g_1 = g_2 = 5000, g_{12} = 10000$ and (ii) the asymmetric (asy) case with $g_1 = 5000, g_2 = g_{12} = 10000$; the numerical results are labeled sym (num) and asym (num), respectively. The theoretical estimates of Feynman (17) and of Fetter (20) for the number and energy, respectively, are also shown.

number of vortices in the second component increases linearly, whereas that in the first component remains zero in the ground state. This phenomenon does not take place in the symmetric case. As a consequence, the number of vortices is reduced in the asymmetric case compared to the symmetric case, viz. Fig. 7(a).

In Figs. 8(a)-(b) we display the numerically obtained number of vortices and the Ω -dependent energy in the rotating frame versus Ω , respectively, for a rotating quasi-2D binary BEC in a square bucket and compare these with the estimate of Feynman for the number of vortices (18) and of Fetter for energy (21), respectively. Actually, the estimate of Feynman for the number of vortices is valid in a large system. In a small system of area 16×16 with boundary as studied in this Letter, a certain area near boundary is excluded from the formation of vortices and the actual number of vortices should be less than the Feynman estimate.

The dynamical stability of the vortex-lattice states of a quasi-2D rotating binary BEC in a circular bucket is tested next. First we consider the symmetric vortex-lattice state of Fig. 3(d) with $g_1 = g_2 = 5000$ and $g_{12} = 10000$. For this purpose we subject this vortex-lattice

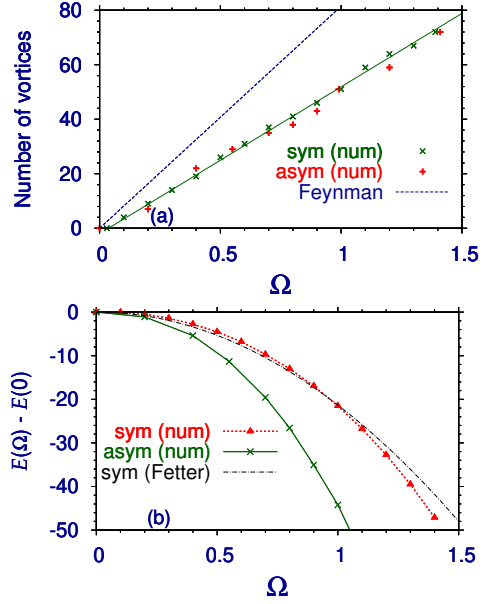


Figure 8: Numerical results for the (a) number of vortices and (b) energy $E(\Omega) - E(0)$ in the rotating frame for a rapidly rotating quasi-2D binary BEC in a square bucket versus angular frequency of rotation Ω for (i) the symmetric (sym) case with $g_1 = g_2 = 5000, g_{12} = 10000$, and (ii) the asymmetric (asy) case with $g_1 = 5000, g_2 = g_{12} = 10000$. The theoretical estimates for the number of vortices (18) by Feynman and for rotational energy (21) by Fetter for the symmetric case are also shown. In (a) the full line through the numerical points is shown to guide the eye.

state obtained by imaginary-time simulation to real-time simulation for a long period of time after changing the rotational frequency Ω from 1.0 to 1.01 at time $t = 0$. The vortex lattice will be destroyed after some time, if the underlying BEC wave function were dynamically unstable. The snapshots of subsequent evolution of the vortex-lattice state is displayed in Fig. 9 at (a) $t = 100$, (b) $t = 200$, (c) $t = 300$, and (d) $t = 400$. The robust nature of the snapshots of the vortex-lattice profiles during real-time evolution upon a small perturbation, as exhibited in Fig. 9, demonstrates the dynamical stability of the vortex lattice in the quasi-2D rotating binary BEC of Fig. 3(d). Next we consider the dynamical stability of the vortex lattice profile of Fig. 4(f) in the asymmetric case with $g_1 = 5000, g_2 = g_{12} = 10000$ and $\Omega = 1.2$. We subject this vortex-lattice state to real-time simulation for a long period of time after changing the rotational frequency Ω from 1.2 to 1.21 at time $t = 0$. The snapshots of subsequent evolution of this vortex-lattice state is displayed in Fig. 9 at (e) $t = 200$, and (f) $t = 400$. The robust nature of the vortex lattice states in (e) and (f) demonstrates the dynamical stability of the

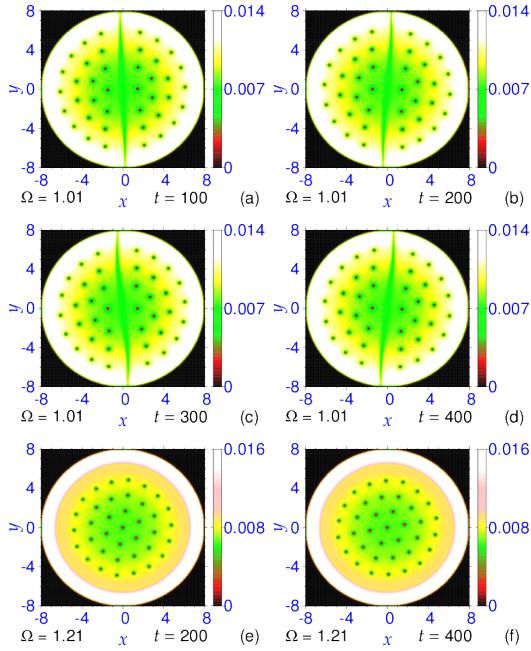


Figure 9: Dynamical evolution of vortex lattice of the rotating BEC in a circular bucket, displayed in Fig. 3(d), during real-time propagation for 400 units of time using the corresponding imaginary-time wave function as input, at times (a) $t = 100$, (b) $t = 200$, (c) $t = 300$, and (d) $t = 400$. During real-time propagation the angular frequency of rotation Ω was changed at $t = 0$ from the imaginary-time value of $\Omega = 1.0$ to 1.01 . The same for the vortex-lattice state of Fig. 4(f) at times (e) $t = 200$ and (f) $t = 400$. During real-time propagation Ω was changed at $t = 0$ from 1.2 to 1.21 .

vortex-lattice state of Fig. 4(f).

The vortex-lattice states of a rotating quasi-2D binary BEC in a square bucket are also found to be dynamically stable. For our demonstration we consider the state of Fig. 5(b) with $g_1 = g_2 = 5000$, $g_{12} = 10000$ and $\Omega = 0.7$ as obtained by imaginary-time evolution and subject it to long-time real-time evolution after changing Ω from 0.7 to 0.71 . In Fig 10 we illustrate the real-time profiles of the vortex-lattice states at times $t =$ (a) 100 , (b) 200 , (c) 300 , and (d) 400 . The robust nature of these states demonstrate the dynamical stability.

4. Summary and Discussion

We studied the generation of spontaneous symmetry-breaking completely phase-separated vortex lattices in a uniform repulsive quasi-2D binary BEC in a circular and a square box. In the examples studied in this Letter, there is no overlap between the component densities of the BEC, so that vortex lattices of the two components are formed in different regions of space, which

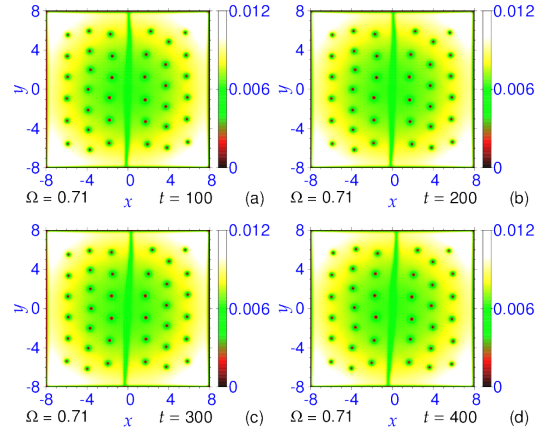


Figure 10: Dynamical evolution of vortex lattice of the rotating BEC in a square bucket, displayed in Fig. 5(b), during real-time propagation for 400 units of time using the corresponding imaginary-time wave function as input, at times (a) $t = 100$, (b) $t = 200$, (c) $t = 300$, and (d) $t = 400$. During real-time propagation the angular frequency of rotation Ω was changed at $t = 0$ from the imaginary-time value of $\Omega = 0.7$ to 0.71 .

is of great phenomenological interest. This will facilitate the experimental study of the vortex lattices of the two components. Such vortex-lattice structure is generated when κ of Eq. (2) is much smaller than unity, e.g., $\kappa \lesssim 0.75$ or so. For larger values of the ratio κ ($0.8 \lesssim \kappa < 1$), although there could be a phase separation for a non-rotating binary BEC, overlapping structure is found under rapid rotation. In this study we fixed this ratio in the symmetric case $g_1 = g_2 = 5000$ as: $\kappa = 0.25$ and study the generation vortex lattice in the case of circular and square buckets. For the asymmetric case $g_1 = 5000$, $g_2 = 10000$ we consider $\kappa = 0.5$. In all cases it was possible to have symmetry-breaking phase-separated vortex lattice under rapid rotation. In the symmetric case, the vortex lattices of the two components lie on fully separated semicircles for a binary BEC in a circular bucket breaking the circular symmetry spontaneously. In case of a square bucket, the phase-separated vortex lattice also breaks the symmetry of the underlying Lagrangian. In the asymmetric case, although the phase separation is complete in a circular bucket, the shapes of the two components are different. In this case, the phase-separated state breaks the symmetry for small Ω , and symmetry is restored for large Ω . We demonstrated dynamical stability of all types of vortex-lattice states by real-time simulation over a long period of time upon a small change in the angular frequency of rotation, viz. Figs. 9 and 10.

The GP equation is valid in the weak-coupling regime for $\kappa \equiv n^{1/3}a \ll 1$. In a recent study we demonstrated that the GP equation is valid for $\kappa < 0.2$ [34]. It is pertinent to ask if the present quasi-2D nonlinearities g of 5000 \sim 10000 correspond to realistic values of experimental parameters, such as atom number N , scattering length a etc, and if the GP equation remains valid for these parameters. The answers are affirmative for a binary mixture of two hyperfine states of $N = 40000$ ^{87}Rb atoms of inter- and intra-species scattering lengths of about 5 nm [35]. For an approximate estimate, we consider a quasi-2D harmonic oscillator trap with trap anisotropy $\omega_x : \omega_y : \omega_z :: 1 : 1 : 100$. For a scaling length $l_0 = 1 \mu\text{m}$, corresponding to a trapping frequency of $\omega \approx 2\pi \times 117$ Hz, the three-dimensional nonlinearity $4\pi Na \approx 2500$ corresponds to a quasi-2D nonlinearity $g_{12} = 2500/\sqrt{2\pi/100} \approx 10000$ [30]. We numerically solved the GP equation in three-dimensions in this case for a nonlinearity of 2500 and found a central density $n \approx 10^3 \mu\text{m}^{-3} = 10^{15} \text{cm}^{-3}$, so that $\kappa = n^{1/3}a \approx 0.05 < 0.2$ guaranteeing the validity of the GP equation. The intra-species scattering length can be reduced by a factor of two by the Feshbach resonance technique [33] to obtain a quasi-2D nonlinearity of 5000. Hence, with present experimental know-how, these phase-separated vortex lattices can be generated and studied in a laboratory using two hyperfine spin states of ^{87}Rb .

Acknowledgements

SKA thanks the Fundação de Amparo à Pesquisa do Estado de São Paulo (Brazil) (Project: 2016/01343-7) and the Conselho Nacional de Desenvolvimento Científico e Tecnológico (Brazil) (Project: 303280/2014-0) for partial support.

References

- [1] L. Onsager, *Nuovo Cimento* 6 (1949) 249.
- [2] R. P. Feynman, *Prog. Low Temp. Phys.* 1 (1955) 17.
- [3] A. A. Abrikosov, *Sov. Phys.-JETP* 5 (1957) 1174.
- [4] A. L. Fetter, *Rev. Mod. Phys.* 81 (2009) 647.
- [5] W. F. Vinen, *Proc. R. Soc. Lond. A* **260** (1961) 218.
- [6] M. J. V. Gordon, G. A. Williams, R. E. Packard, *J. Phys. (Paris)* 39 (1978) C6-172.
- [7] M. H. Anderson, J. R. Ensher, M. R. Matthews, C. E. Wieman, and E. A. Cornell, *Science* 269 (1995) 198; K. B. Davis, M. -O. Mewes, M. R. Andrews, N. J. van Druten, D. S. Durfee, D. M. Kurn, and W. Ketterle, *Phys. Rev. Lett.* 75 (1995) 3969.
- [8] K. W. Madison, F. Chevy, W. Wohlleben, and J. Dalibard, *Phys. Rev. Lett.* 84 (2000) 806; M. R. Matthews, B. P. Anderson, P. C. Haljan, D. S. Hall, M. J. Holland, J. E. Williams, C. E. Wieman, and E. A. Cornell, *Phys. Rev. Lett.* 83 (1999) 3358;
- [9] J. R. Abo-Shaeer, C. Raman, J. M. Vogels, and W. Ketterle, *Science* 292 (2001) 476; P. C. Haljan, B. P. Anderson, I. Coddington, and E. A. Cornell, *Phys. Rev. Lett.* 86 (2001) 2922.
- [10] D. L. Feder, C. W. Clark, B. I. Schneider, *Phys. Rev. Lett.* 82 (1999) 4956; A. A. Penckwitt, R. J. Ballagh, C. W. Gardiner, *Phys. Rev. Lett.* 89 (2002) 260402; M. Tsubota, K. Kasamatsu, M. Ueda, *Phys. Rev. A* 65 (2002) 023603; C. Lobo, A. Sinatra, Y. Castin, *Phys. Rev. Lett.* 92 (2004) 020403.
- [11] E. P. Gross, *Nuovo Cimento* 20 (1961) 454; L. P. Pitaevskii, *Sov. Phys. JETP* 13 (1961) 451.
- [12] T. P. Meyrath, F. Schreck, J. L. Hanssen, C.-S. Chuu, M. G. Raizen, *Phys. Rev. A* 71 (2005) 041604(R); J. J. P. van Es, P. Wicke, A. H. van Amerongen, C. Rétif, S. Whitlock, N. J. van Druten, *J. Phys. B* 43 (2010) 155002.
- [13] N. Navon, A. L. Gaunt, R. P. Smith, Z. Hadzibabic, *Nature* 539 (2016) 72; S. J. Garratt, C. Eigen, J. Zhang, P. Turzák, R. Lopes, R. P. Smith, Z. Hadzibabic, N. Navon, *Phys. Rev. A* 99 (2019) 021601(R); A. L. Gaunt, T. F. Schmidutz, I. Gotlibovych, R. P. Smith, Z. Hadzibabic, *Phys. Rev. Lett.* 110 (2013) 200406; R. Saint-Jalm, P. C. M. Castilho, É. Le Cerf, B. Bakkali-Hassani, J. L. Ville, S. Nascimbene, J. Beugnon, J. Dalibard, *Phys. Rev. X* 9 (2019) 021035.
- [14] S. K. Adhikari, *J. Phys.: Condens. Matter* 31 (2019) 275401.
- [15] S. K. Adhikari, *Physica E* 115 (2020) 113713.
- [16] V. Schweikhard, I. Coddington, P. Engels, S. Tung, E. A. Cornell, *Phys. Rev. Lett.* 93 (2004) 210403.
- [17] R. K. Kumar, L. Tomio, B. A. Malomed, A. Gammal, *Phys. Rev. A* 96 (2017) 063624; N. Ghazanfari, A. Keleş, M. Ö. Oktel, *Phys. Rev. A* 89 (2014) 025601.
- [18] K. Kasamatsu, K. Sakashita, *Phys. Rev. A* 97 (2018) 053622.
- [19] A. E. Leanhardt, Y. Shin, D. Kielpinski, D. E. Pritchard, W. Ketterle, *Phys. Rev. Lett.* 90 (2003) 140403.
- [20] M. Cipriani, M. Nitta, *Phys. Rev. Lett.* 111 (2013) 170401; S. Gautam, S. K. Adhikari, *Phys. Rev. A* 93 (2016) 013630.
- [21] S. K. Adhikari, *Commun. Nonlinear Sci. Numer. Simulat.* 71 (2019) 212.
- [22] E. J. Mueller, T. -L. Ho, *Phys. Rev. Lett.* 88 (2002) 180403. R. Barnett, G. Refael, M. A. Porter, H. P. Buchler, *New J. Phys.* 10 (2008) 043030. R. Wei, E. Mueller, *Phys. Rev. A* 84 (2011) 063611. P. Kuopanportti, J. A. M. Huhtamäki, M. Möttönen, *Phys. Rev. A* 85 (2012) 043613.
- [23] K. Kasamatsu, M. Tsubota, M. Ueda, *Phys. Rev. Lett.* 91 (2003) 150406.
- [24] D. S. Hall, M. R. Matthews, J. R. Ensher, C. E. Wieman, E. A. Cornell, *Phys. Rev. Lett.* 81 (1998) 1539.
- [25] See, for example, V.P. Mineev, *Sov. Phys.-JETP* 40 (1975) 132; E. Timmermans, *Phys. Rev. Lett.* 81 (1998) 5718; K. L. Lee, N. B. Jorgensen, I-K. Liu, L. Wacker, J. J. Arlt, N. P. Proukakis, *Phys. Rev. A* 94 (2016) 013602.
- [26] C. J. Pethick, H. Smith, *Bose-Einstein Condensation in Dilute Gases* (2002) (Cambridge University Press, Cambridge).
- [27] K. Kasamatsu, M. Tsubota, M. Ueda, *Int. J. Mod. Phys. B* 19 (2005) 1835. H. Wang, *J. Sci. Comput.* 38 (2009) 149.

- P. Mason, A. Aftalion, Phys. Rev. A 84 (2011) 033611.
- [28] P. Muruganandam, S. K. Adhikari, Comput. Phys. Commun. 180 (2009) 1888.
L. E. Young-S., P. Muruganandam, S. K. Adhikari, V. Lončar, D. Vudragović, A. Balaž, Comput. Phys. Commun. 220 (2017) 503;
L. E. Young-S., D. Vudragović, P. Muruganandam, S. K. Adhikari, A. Balaž, Comput. Phys. Commun. 204 (2016) 209;
- [29] L. D. Landau, E. M. Lifshitz, *Mechanics* (Pergamon Press, Oxford, 1960), section 39.
- [30] L. Salasnich, A. Parola, L. Reatto, Phys. Rev. A 65 (2002) 043614.
- [31] D. Vudragović, I. Vidanović, A. Balaž, P. Muruganandam, S. K. Adhikari, Comput. Phys. Commun. 183 (2012) 2021.
- [32] R. Kishor Kumar, V. Lončar, P. Muruganandam, S. K. Adhikari, A. Balaž, Comput. Phys. Commun. 240 (2019) 74.
- [33] S. Inouye, M. R. Andrews, J. Stenger, H.-J. Miesner, D. M. Stamper-Kurn, W. Ketterle, Nature 392 (1998) 151.
- [34] S. Gautam and S. K. Adhikari, Phys. Rev. A 100 (2019) 023626.
- [35] D. S. Hall, M. R. Matthews, J. R. Ensher, C. E. Wieman, and E. A. Cornell, Phys. Rev. Lett. **81**, 1539 (1998); H. M. J. M. Boesten, C. C. Tsai, J. R. Gardner, D. J. Heinzen, and B. J. Verhaar, Phys. Rev. A **55**, 636 (1997).